Titanium Trisulfide Nanosheets and Nanoribbons for Field Emission-Based Nanodevices

Pawbake, Amit S.; Khare, Ruchita T.; Island, Joshua O.; Flores, Eduardo; Ares, Jose R.; Sanchez, Carlos; Ferrer, Isabel J.; Van Der Zant, Herre S.J.; Castellanos-Gomez, Andres; More Authors

DOI
10.1021/acsanm.2c03460

Publication date
2023

Document Version
Final published version

Published in
ACS Applied Nano Materials

ACS APPLIED NANO MATERIALS

www.acsanm.org Article

Titanium Trisulfide Nanosheets and Nanoribbons for Field Emission-Based Nanodevices

Amit S. Pawbake,[¶] Ruchita T. Khare,[¶] Joshua O. Island, Eduardo Flores, Jose R. Ares, Carlos Sanchez, Isabel J. Ferrer, Mahendra Pawar, Otakar Frank, Mahendra A. More,* Herre S. J. van der Zant, Andres Castellanos-Gomez,* and Dattatray J. Late*

Cite This: *ACS Appl. Nano Mater.* 2023, 6, 44–49 Read Online

ACCESS | Metrics & More | Article Recommendations

ABSTRACT: The field emission (FE) properties of TiS_3 nanosheets and nanoribbons, synthesized by direct sulfuration of bulk titanium, are investigated. The nanosheets show an enhanced FE behavior with a low turn-on field of ~0.3 V/μm, required for drawing an emission current density of ~10 μA/cm^2. Interestingly, the TiS_3 nanosheet emitter delivered a large emission current density of ~0.9 mA/cm^2 at a relatively low applied electric field of ~0.4 V/μm. We have estimated the values of the field enhancement factor (β), which are found to be ~5 × 10^4 for the TiS_3 nanosheet emitter and ~4 × 10^3 for the nanoribbon emitter. We attribute the superior FE performance to the presence of atomically sharp edges and the reduced thickness of TiS_3, as reflected in the high value of β. In fact, the nanosheet sample presents a higher density of ultrathin layers (~12 nm-thick), and thus, they have a larger edge to volume ratio than the nanoribbon samples (which are ~19 nm-thick). The superior FE behavior of TiS_3 nanosheets over nanoribbons makes them a propitious field emitter and can be utilized for various FE-based applications, demanding large emission currents and lower operational voltages. Moreover, the FE current stability recorded on these samples confirms their promising performance. Thus, the present investigation brings out a great promise of TiS_3 nanosheets and nanoribbons as field emitters for vacuum nanoelectronics devices.

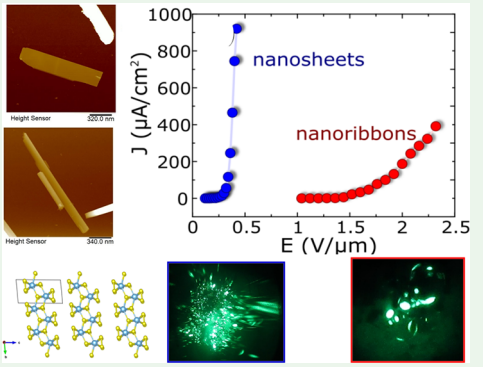

KEYWORDS: *TiS_3, nanosheets, nanoribbon, field emission, current stability*

INTRODUCTION

The synthesis, characterization, and technological applications of one-dimensional (1D) nanostructures, namely, nanorods, nanowires, nanoneedles, and nanobelts, have been a subject of study over the past decade due to their high aspect ratios.[1] One of the lesser explored 1D nanostructures is the nanoribbon structure (partly 1D), which can be used for both fundamental research and technological applications.[1−3] However, the large-scale exercise of 1D nanoforms for device applications still faces challenges and opportunities, such as assembling them in an ordered array form or manufacturing them with uniform dimensions and narrow size dispersion. These limitations, to a certain extent, can be overcome by two-dimensional (2D) nanostructures as their geometries are favorable for designing and realization of novel devices facilitating integration with the present solid-state electronic devices (metal−oxide−semiconductor-based field effect transistors (FETs))[4] To exemplify, very recently, Jia *et. al* comprehensively reviewed the state-of-the-art fabrication techniques for the on-chip integration of 2D materials, along with the current challenges and future perspectives.[5] Furthermore, reproducibility and uniformity of dimensions can be maintained for the 2D structured materials. In anticipation, layered nanostructures have received immense research interest in the past few years owing to their exceptional properties.[4,5] Particularly, transition metal dichalcogenides (TMDCs), identified as semiconducting 2D layered materials, possess exceptional physicochemical properties and have been realized for many technological applications including optoelectronic devices,[6] gas sensing,[7] and energy storage devices.[8]

Field emission (FE), emission of electrons from a condensed matter phase into vacuum under the application of a strong electrostatic field, has facilitated performance improvement of various vacuum microelectronic devices, particularly the electron microscopes. With the advent of 1D nanostructures, "planar" field emitters (an assembly of nanostructures

Received: August 6, 2022
Accepted: December 19, 2022
Published: January 4, 2023

https://doi.org/10.1021/acsanm.2c03460
ACS Appl. Nano Mater. 2023, 6, 44−49

deposited in thin film form on a suitable substrate) are found to be advantageous over conventional single "micro-tip" emitters. Owing to the high "aspect ratio" of the 1D/2D nanostructures, the planar emitters exhibit competency to deliver very high emission current densities at relatively lower applied voltages. The 1D/2D nanostructure-based field emitters have been realized for development of novel nanoelectronics scheme for space applications based on vacuum field emission transistors (VFETs).[4] Although, in principle, every 1D/2D nanostructure possessing a high aspect ratio shows potential as a field emitter and consequently has been investigated, 2D nanostructure-based emitters like graphene,[9] reduced graphene oxide, and their analogous 2D materials (the TMDCs), are observed to possess promising FE behavior.[10] To exemplify, Bartolomeo *et al.* investigated the transfer characteristics of a VFET made up of a single layer WSe_2 on a SiO_2/Si substrate, which exhibited excellent emission stability (fluctuations ≤5%) during continuous operation for more than 20 h.[11] These interesting results have motivated further work on alike layered structures, predominantly TMDCs.[11−16]

The transition metal trichalcogenides (TMTCs) represent an important class of materials possessing a unique set of properties and potential for technological applications. Among various TMTCs, titanium trisulfide (TiS_3) is an *n*-type semiconductor with an optical bandgap of ∼1 eV.[18] It forms sheets held together by van der Waals forces by parallel chains of triangular prisms. Due to these parallel chains, the material's conductivity is anisotropic between the in planes of the "*a*" and "*b*" axes, resulting in a quasi-1D structure.[17] The thin films of TiS_3 can be obtained by direct reaction of titanium and sulfur in a sealed ampoule.[18] Despite possessing exotic properties and potential for applications in field emission, characterization of TiS_3 nanostructures has not hitherto been attempted.

Here, we report the field emission behavior of both the partial 1D and 2D nanoforms of TiS_3, nanoribbons and nanosheets, respectively. The sharp tip apex as well as the ultrathin/sharp edges of nanoribbons and nanosheets significantly enhance the local electric field, thereby reducing the operational voltages noticeably. The observed values of turn-on field (∼0.3 V/μm, for an emission current density of ∼10 μA/cm^2) and field required to extract a maximum emission current density (∼0.3 V/μm, for emission current density of ∼10 μA/cm^2) are found to be superior to the earlier reports on 2D nanostructure emitters. Thus, the TiS_3 nanosheets and nanoribbons may serve as propitious materials for practical applications in field emission-based devices, demanding large emission current densities and lower operational voltages.

RESULTS AND DISCUSSION

The schematic illustration of a solid−gas reaction method used for the synthesis of TiS_3 nanosheets and nanoribbons is depicted in Figure 1a. The schematic of a crystal structure for TiS_3 is shown in Figure 1b. As compared to the *a*-axis, the bond length between titanium and sulfur is shorter along the *b*-axis. As a result, strong anisotropic optical and electrical properties are obtained by creating highly conducting chains. Figure 1c represents the schematic illustration of generation of FE images from the TiS_3 emitter. During field emission, electrons emit from the surface of the cathode sample at a negatively biased potential. The emergence of an image potential at the boundary lowers the surface barrier height, resulting in the electron emission occurring easily. The

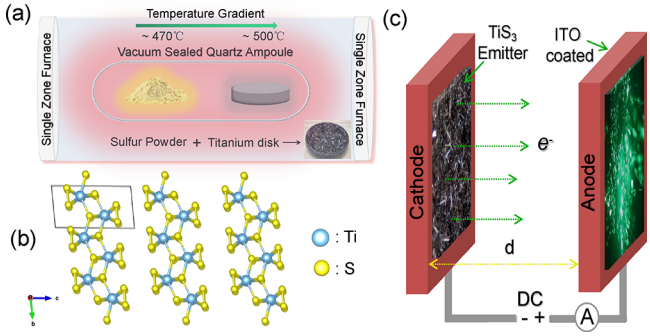

Figure 1. Schematic of the (a) vapor transport method involved in the synthesis of TiS_3 nanoribbons. The inset shows an actual zoomed-in view of a sulfureted titanium disk. (b) Crystal structure of TiS_3. The central Ti metal atoms (light blue color) are covalently bonded to six S atoms (yellow color), forming a trigonal prism. These prisms share triangular faces to form 1D chains (shown by dashed lines). (c) Schematic illustration of generation of FE images from the TiS_3 emitter.

crystalline nature of the synthesized nanoribbons and nanosheets was confirmed by Raman spectroscopic analysis. Figure 2a and 1b show the Raman spectra of TiS_3 nanosheets and

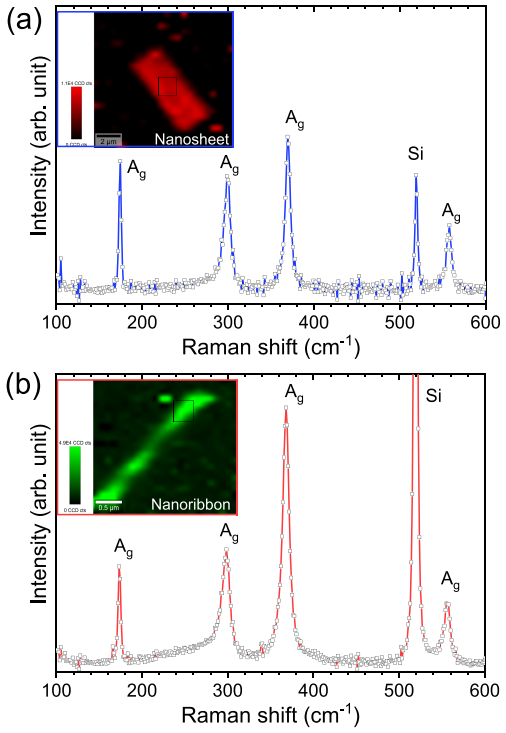

Figure 2. Comparative Raman spectra of TiS_3 (a) nanosheets and (b) nanoribbon measured with 532.5 nm laser line. The inset shows the respective Raman map, which is generated from the A_g Raman peak centered at ∼370 cm^{-1}.

nanoribbons, respectively, and the insets show the respective Raman mapping images. We observed four intense A_g Raman phonon modes around 175, 300, 370, and 557 cm^{-1}, and these are in good agreement with earlier reports.[19,21] The Raman peak at ∼520 cm^{-1} is a signature of a silicon substrate. In the Raman spectrum, Raman-active phonon modes oscillate along the *c*-axis perpendicular to the quasi-1D chain, whereas B_g phonon modes involving atomic displacement along the chain

https://doi.org/10.1021/acsanm.2c03460
ACS Appl. Nano Mater. 2023, 6, 44−49

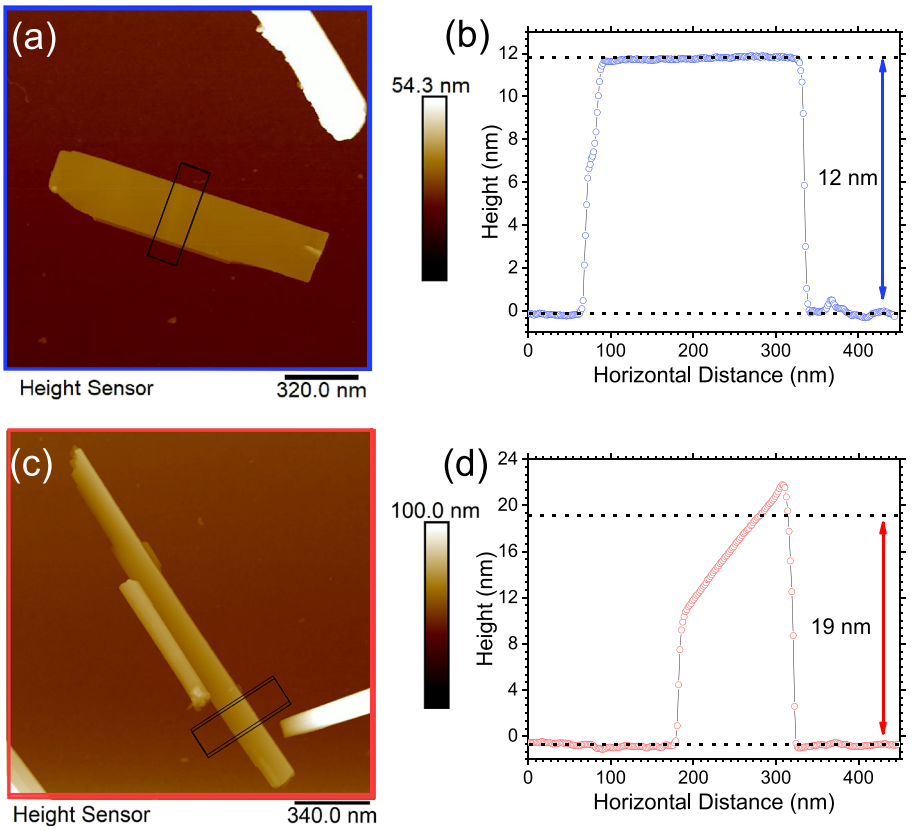

Figure 3. AFM images and AFM height profiles for typical (a, b) TiS_3 nanosheet and (c, d) TiS_3 nanoribbon samples.

(*b*-axis) are weak. The increase in lattice spacing of the nanosheets can be attributed to the increased lattice strain; hence, slight intensity and peak position changes are observed in Raman spectra. The detailed lattice vibrational properties and their physical significance were discussed earlier.[19,21,22]

Figure 3a–d shows the AFM images and AFM step height profiles for TiS_3 nanosheet and nanoribbon samples. The AFM images and height profiles show the typical thicknesses of the nanosheet and nanoriboon, ∼12 and ∼19 nm. The thickness measurements were done on several flakes for the nanoribbons, varying from ∼13 to ∼60 nm, and for the nanosheets, varying from ∼0.8 to ∼30 nm in thickness.[20] The X-ray diffraction,[20] AFM[20], and transmission[21] and scanning electron microscopy analyses of the TiS_3 nanosheets and nanoribbons are detailed in our previous work.[19−21]

For the field emission study of TiS_3 specimens (see the Methods and Experimental Section), which were pasted on a copper stub in two different experiments runs: one for the nanosheet specimen and another one for the nanoribbon specimen, a modified Fowler–Nordheim (F-N) equation[23,24] was used for the analysis of field emission current density versus applied electric field data from the F-N plot for TiS_3 nanoribbon and nanosheet emitters. The modified F-N equation is as follows:

$$J = \lambda_M a \phi^{-1} E^2 \beta^2 \exp\left(-\frac{b\phi^{3/2}}{\beta E} v_F\right) \quad (1)$$

where λ_M is the macroscopic pre-exponential correction factor, J is the emission current density, E is the applied average electric field (surface field), a and b are constants ($a = 1.54 \times 10^{-6}$ AeV/V^2, $b = 6.83$ eV$^{-3/2}$Vnm^{-1}), ϕ is the work function of the emitter, β is the field enhancement factor, and v_F (correction factor) is a particular value of the principal Schottky–Nordheim barrier function v. Figure 4a shows the comparative J–E plot for the TiS_3 nanosheet and nanoribbon samples. The values of turn-on and threshold field are defined as the applied electric field required for drawing emission current densities of 10 and 100 μA/cm^2, respectively. The turn-on field for the TiS_3 nanosheets and nanoribbons are found to be ∼0.3 V/μm and ∼1.4 V/μm, respectively. The remarkably low turn-on field of TiS_3 nanosheets can be attributed to the thin nature and sharp edges of the nanosheets as compared with that of the nanoribbon sample as evident from the AFM images and height profiles (Figure 3). Furthermore, the threshold fields for TiS_3 nanosheets and nanoribbons are found to be ∼0.4 V/μm and ∼1.8 V/μm, respectively. The nanostructured geometry of TiS_3 materials supports (i) a reduced turn-on electric field for the onset of field emission and (ii) a large field-enhancement factor that is attributed to the presence of "sharp nanometric size protrusions" on the edges of the nanostructures. The maximum emission current densities of ∼0.9 mA/cm^2 were drawn from TiS_3 nanosheets at an applied electric field of ∼0.4 V/μm. For the TiS_3 nanoribbon sample, the current density increases rapidly with the applied electric field and reaches a maximum value of ∼0.4 mA/cm^2 at an applied field of ∼2.3 V/μm. The corresponding F-N plot is shown in Figure 4b. The F-N curve exhibits a non-linear behavior with saturation at a higher applied electric field. The slope of the F-N curves gives the value of the field enhancement ratio (β) by the equation

$$\beta = \frac{(-6.8 \times 10^3)\phi^{3/2}}{m} \quad (2)$$

https://doi.org/10.1021/acsanm.2c03460
ACS Appl. Nano Mater. 2023, 6, 44−49

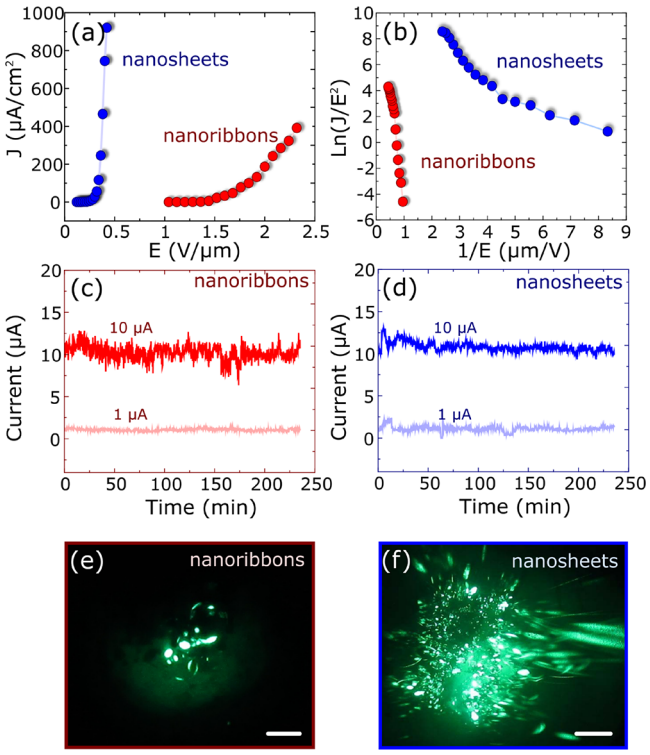

Figure 4. Field emission investigations of TiS_3 nanosheets and nanoribbons. (a) J–E characteristics. (b) Comparative F-N plot showing non-linear behavior indicating the emission current from the semiconducting emitter. Field emission current stability (I–t) plots for (c) nanoribbon and (d) nanosheet emitters. Field emission images recorded at (e) ∼0.3 mA/cm^2 for TiS_3 nanoribbons and (f) ∼0.8 mA/cm^2 for TiS_3 nanosheets. The scale bar in (e and f) depicts 6 mm length.

In the present case, β was calculated by taking the value of ϕ for TiS_3 as 4.6 eV.[24,25] The field enhancement factors β for TiS_3 nanosheets and nanoribbons were calculated by using eq 2 and are found to be ∼5 × 10^4 and ∼4 × 10^3, respectively. Such a high value of β for the nanosheets is due to the presence of sharp nanometric size protrusions on their edges, which are responsible for the enhanced field emission behavior. The low value of turn-on and threshold field can be attributed to the extremely high value of β, suggesting TiS_3 nanosheets and nanoribbons as promising field emitters. The observed high value of the field enhancement factor is attributed to the presence of sharp protrusions/nanosized features of the emitter surface; the local electric field at the apex of such protrusions gets enhanced. In fact, the observed higher emission current in the TiS_3 nanosheet sample with respect to the nanoribbon ones aligns well with the higher edge to volume ratio for the nanosheet sample, thereby explaining the enhanced field emission for nanosheet. The enhanced field emission behavior of nanosheets over nanoribbons can also be explained with the help of phonon-assisted electron emission, which is peculiar for materials with monatomic thickness. The FE behaviors of both nanoforms are compared with the existing 1D and 2D materials, and their heterostructures and are given in Table 1. Table 2 shows the comparative values of nanoribbons and nanosheets of TiS_3 studied in the present case.

Table 2. Field Emission Properties of TiS_3 Nanosheets and Nanoribbons

TiS_3 morphology	turn on field (V/μm) at 1 μA/cm^2	turn on field (V/μm) at 10 μA/cm^2	maximum emission current density and field	field enhancement factor (β)
nanosheets	∼0.2	∼0.3	∼0.9 mA/cm^2 at ∼0.4 V/μm	∼5 × 10^4
nanoribbons	∼1.3	∼1.4	∼0.4 mA/cm^2 at ∼2.3 V/μm	∼4 × 10^3

Furthermore, the emission stability is a prior requirement for a material to be the best field emitter. The current stabilities of TiS_3 nanoribbons and nanosheets were recorded at preset values of 1 and 10 μA for about 3 h, and the corresponding current vs time (I–t) curves are shown in Figure 4c,d, respectively. At a lower preset value, the current stability is fairly good, whereas at a higher emission current, small fluctuations can be observed. They result from the adsorption/desorption of residual gas molecules on/from the emitter surface.[32,33] Figure 4e,f shows the field emission micrographs of the nanoribbon and nanosheet emitter samples, respectively.

Table 1. Comparison of Field Emission Properties of Reported 1D and 2D Nanomaterials

dimensions of nanofield emitters	field emitter material	synthesis route of material	turn on field (V/μm) at 10 μA/cm^2	field enhancement factor	stability and fluctuations	reference
1D	CdS nanowires	thermal evaporation	9	550		26
	ZnS nanowires	thermal evaporation	2.9	2700	<0.8%	27
	Si nanocone	RF sputtering	13			28
	graphene nanoribbon	unzipping MWCNTs	5.8	818	3 h, <7%	29
	TiS_3 nanoribbons	sulfuration of titanium	∼1.4	∼4 × 10^3	3 h, <8%	present work
2D (nanosheets)	MoS_2	solution method	3.5	1138		12
	WS_2	hydrothermal	4.4	2468		15
	SnS_2	hydrothermal	5.9	3200		16
	VS_2	hydrothermal	5.01	2500		14
	CuS	solvothermal	2.05	7261		30
	TiS_3 nanosheets	sulfuration of titanium	∼0.3	∼5 × 10^4	3 h, <10%	present work
3D nanoheteroarchitecture	GdB_6	PLD	2.3 at 1 μA/cm^2	2860		31

https://doi.org/10.1021/acsanm.2c03460
ACS Appl. Nano Mater. 2023, 6, 44−49

The field emission micrograph reflects the symmetry and work function variation of TiS_3nanosheet and nanoribbon emitter surfaces.

CONCLUSIONS

In conclusion, the low turn-on fields of ∼0.3 and ∼ 1.4 V/μm were observed in the case of TiS_3 nanosheet and nanoribbon samples, respectively, required to draw an emission current density of ∼1 μA/cm^2. Interestingly, the high field enhancement factor of ∼5 × 10^4 was observed for the TiS_3 nanosheet sample, which indicates field emission current from nanometer-scaled features. The field emission current stability for TiS_3 nanosheet and nanoribbon samples indicates the great potential for field emission-based device applications. The low turn-on fields and high field enhancement factors can make the TiS_3 nanosheets and nanoribbons potential candidates for field emission-based nanodevices.

METHODS AND EXPERIMENTAL SECTION

TiS_3 nanoribbons and nanosheets were synthesized by heating sulfur powder (99.99% purity) in a vacuum-sealed ampoule with Ti powder at 550 and 400 °C to provide sulfur gas for the solid−gas reaction.[19−21] The AFM tapping mode images were recorded using a Bruker Dimension Icon instrument. Raman spectra and mapping on TiS_3 nanostructures were recorded in backscattering geometry using the WITec alpha 300 R system with 532.5 nm excitation and 0.5 mW power. The field emission experiments of TiS_3 nanoribbons and nanosheets were carried out in separate experimental batches in a UHV chamber evacuated to a base pressure of ∼1 × 10^{-8} mbar in the close proximity setup consists of a specimen (TiS_3 nanosheets or nanoribbons that were sprinkled over carbon tape size ∼5 mm × 5 mm) as a cathode and copper rod as an anode. The detailed description of the FE system is reported earlier.[31,32]

AUTHOR INFORMATION

Corresponding Authors

Mahendra A. More − *Center for Advanced Studies in Materials Science and Condensed Matter Physics, Department of Physics, University of Pune, Pune 411007, India*; Email: mam@physics.unipune.ac.in

Andres Castellanos-Gomez − *Materials Science Factory, Instituto de Ciencia de Materiales de Madrid (ICMM-CSIC), Madrid E-28049, Spain*; orcid.org/0000-0002-3384-3405; Email: andres.castellanos@csic.es

Dattatray J. Late − *Centre for Nanoscience and Nanotechnology, Amity University Maharashtra, Mumbai, Panvel 410206, India*; orcid.org/0000-0003-3007-7220; Email: datta099@gmail.com, djlate@mum.amity.edu

Authors

Amit S. Pawbake − *J. Heyrovský Institute of Physical Chemistry, Czech Academy of Sciences, 182 23 Prague, Czech Republic*; orcid.org/0000-0002-6345-489X

Ruchita T. Khare − *Center for Advanced Studies in Materials Science and Condensed Matter Physics, Department of Physics, University of Pune, Pune 411007, India*

Joshua O. Island − *Department of Physics and Astronomy, University of Nevada Las Vegas, Las Vegas, Nevada 89154, United States*; orcid.org/0000-0002-6074-9414

Eduardo Flores − *Departamento de Física Aplicada, Centro de Investigación y de Estudios Avanzados, Unidad Mérida, 97310 Mérida, Yucatan, México*

Jose R. Ares − *Materials of Interest in Renewable Energies Group (MIRE Group), Dpto. de Física de Materiales, Universidad Autónoma de Madrid (UAM), 28049 Madrid, Spain*; orcid.org/0000-0001-5238-1800

Carlos Sanchez − *Materials of Interest in Renewable Energies Group (MIRE Group), Dpto. de Física de Materiales, Universidad Autónoma de Madrid (UAM), 28049 Madrid, Spain*; orcid.org/0000-0001-9816-4537

Isabel J. Ferrer − *Materials of Interest in Renewable Energies Group (MIRE Group), Dpto. de Física de Materiales, Universidad Autónoma de Madrid (UAM), 28049 Madrid, Spain*; orcid.org/0000-0003-2125-5865

Mahendra Pawar − *Physical & Materials Chemistry Division, CSIR-National Chemical Laboratory, Pune 411008, India*

Otakar Frank − *J. Heyrovský Institute of Physical Chemistry, Czech Academy of Sciences, 182 23 Prague, Czech Republic*; orcid.org/0000-0002-9661-6250

Herre S. J. van der Zant − *Kavli Institute of Nanoscience, Delft University of Technology, 2628 CJ Delft, The Netherlands*; orcid.org/0000-0002-5385-0282

Complete contact information is available at: https://pubs.acs.org/10.1021/acsanm.2c03460

Author Contributions

¶A.S.P. and R.T.K. contributed equally to this work

Author Contributions

D.J.L. and A.C.-G. conceptualized this project. A.S.P., R.T.K., J.O.I., E.F., J.R.A., C.S., I.J.F., M.P., O.F., M.A.M., H.S.J.Z, A.C.-G., and D.J.L. prepared and characterized the materials. A.S.P. and R.T.K. performed the field emission measurements of TiS_3 nanoribbon and nanosheet samples and processed the data. A.S.P prepared all schematic representations. All authors analyzed and discussed the data. M.A.M., A.C.-G., and D.J.L. wrote the first draft of the manuscript, with all authors commenting and editing the manuscript.

Notes

The authors declare no competing financial interest.

ACKNOWLEDGMENTS

D.J.L. would like to thank Prof. C. N. R. Rao (FRS), JNCASR and ICMS Bangalore (India) and Prof. Vinayak P. Dravid (Northwestern University, USA) for encouragement and support. The authors thank Director CSIR-National Chemical Laboratory Pune (India) for the support. This work was supported by the Dutch Organization for Fundamental research (NWO/FOM). Mire group acknowledges F. Moreno for technical support. O.F. acknowledges the support of the Czech ScienceFoundation Project No. 20-08633X.

REFERENCES

(1) Island, J. O.; Molina-Mendoza, A. J.; Barawi, M.; Biele, R.; Flores, E.; Clamagirand, J. M.; Ares, J. R.; Sánchez, C.; van der Zant, H. S. J.; D'Agosta, R.; Ferrer, I. J.; Castellanos-Gomez, A. Electronics and Optoelectronics of Quasi-1D Layered Transition Metal Trichalcoge-nides. *2D Mater.* **2017**, *4*, 22003.

(2) Hughes, W. L.; Wang, Z. L. Nanobelts as nanocantilevers. *Appl. Phys. Lett.* **2003**, *82*, 2886.

(3) Arnold, M. S.; Avouris, P.; Pan, Z. W.; Wang, Z. L. Field-effect transistors based on single semiconducting oxide nanobelts. *J. Phys. Chem. B* **2003**, *107*, 659−663.

(4) Han, J. W.; Moon, D. I.; Meyyappan, M. Cofabrication of vacuum field emission transistor (VFET) and MOSFET. *IEEE Trans. Nanotechnol.* **2014**, *13*, 464−468.

(5) Jia, L.; Wu, J.; Zhang, Y.; Qu, Y.; Jia, B.; Chen, Z.; Moss, D. J. Fabrication Technologies for the On-Chip Integration of 2D Materials. *Small Methods* **2022**, *6*, 2101435.
(6) Ganatra, R.; Zhang, Q. Few-Layer MoS_2: A Promising Layered Semiconductor. *ACS Nano* **2014**, *8*, 4074−4099.
(7) Wu, S. X.; Zeng, Z. Y.; He, Q. Y.; Wang, Z. J.; Wang, S. J.; Du, Y. P.; Yin, Z. Y.; Sun, X. P.; Chen, W.; Zhang, H. Electrochemically Reduced Single-Layer MoS2 Nanosheets: Characterization, Properties and Sensing Applications. *Small* **2012**, *8*, 2264−2270.
(8) Huang, X.; Qi, X. Y.; Boey, F.; Zhang, H. *Chem. Soc. Rev.* **2012**, *41*, 666.
(9) Ye, D.; Moussa, S.; Ferguson, J. D.; Baski, A. A.; El-Shall, M. S. Highly Efficient Electron Field Emission from Graphene Oxide Sheets Supported by Nickel Nanotip Arrays. *Nano Lett.* **2012**, *12*, 1265−1268.
(10) Li, Y. B.; Bando, Y.; Golberg, D. MoS_2 Nanoflowers and Their Field-Emission Properties. *Appl. Phys. Lett.* **2003**, *82*, 1962−1964.
(11) Bartolomeo, A.; Urban, F.; Passacantando, M.; McEvoy, N.; Peters, L.; Iemmo, L.; Luongo, G.; Romeo, F.; Giubileo, F. A WSe_2 Vertical Field Emission Transistor. *Nanoscale* **2019**, *11*, 1538−1548.
(12) Kashid, R. V.; Late, D. J.; Chou, S. S.; Huang, Y.-K.; De, M.; Joag, D. S.; More, M. A.; Dravid, V. P. Enhanced field-emission behavior of layered MoS_2 sheets. *Small* **2013**, *9*, 2730−2734.
(13) Song, C.; Yu, K.; Yin, H.; Fu, H.; Zhang, Z.; Zhang, N.; Zhu, Z. Highly efficient field emission properties of a novel layered VS2/ZnO nanocomposite and flexible VS_2 nanosheet. *J. Mater. Chem. C* **2014**, *2*, 4196−4202.
(14) Rout, C. S.; Khare, R.; Kashid, R. V.; Joag, D. S.; More, M. A.; Lanzillo, N. A.; Washington, M.; Nayak, S. K.; Late, D. J. Metallic Few-Layer Flowerlike VS_2 Nanosheets as Field Emitters. *Eur. J. Inorg. Chem.* **2014**, *2014*, 5331−5336.
(15) Rout, C. S.; Joshi, P. D.; Kashid, R. V.; Joag, D. S.; More, M. A.; Simbeck, A. J.; Washington, M.; Nayak, S. K.; Late, D. J. Superior field emission properties of layered WS_2-RGO nanocomposites. *Sci. Rep.* **2013**, *3*, 3282.
(16) Rout, C. S.; Joshi, P. D.; Kashid, R. V.; Joag, D. S.; More, M. A.; Simbeck, A. J.; Washington, M.; Nayak, S. K.; Late, D. J. Enhanced field emission properties of doped graphene nanosheets with layered SnS_2. *Appl. Phys. Lett.* **2014**, *105*, No. 043109.
(17) Gorlova, I. G.; Zybtsev, S. G.; Pokrovskii, V. Y.; Bolotina, N. B.; Verin, I. A.; Titov, A. N. Nonlinear Conductivity of Quasi-One-Dimensional Layered Compound TiS_3. *Phys. B* **2012**, *407*, 1707−1710.
(18) Murray, J. L. The S−Ti (Sulfur-Titanium) System. *Bull. Alloy Phase Diagrams* **1986**, *7*, 156−163.
(19) Mishra, K. K.; Ravindran, T. R.; Island, J. O.; Flores, E.; Ares, J. R.; Sanchez, C.; Ferrer, I. J.; van der Zant, H. S. J.; Pawbake, A.; Kanawade, R.; Castellanos-Gomez, A.; Late, D. J. Raman Fingerprint of Pressure-Induced Phase Transitions in TiS_3 Nanoribbons: Implications for Thermal Measurements under Extreme Stress Conditions. *ACS Appl. Nano Mater.* **2020**, *3*, 8794−8802.
(20) Island, J. O.; Barawi, M.; Biele, R.; Almazán, A.; Clamagirand, J. M.; Ares, J. R.; Sánchez, C.; van der Zant, H. S. J.; Álvarez, J. V.; D'Agosta, R.; et al. TiS_3 Transistors with Tailored Morphology and Electrical Properties. *Adv. Mater.* **2015**, *27*, 2595−2601.
(21) Pawbake, A. S.; Island, J. O.; Flores, E.; Ares, J. R.; Sanchez, C.; Ferrer, I. J.; Jadkar, S. R.; van der Zant, H. S. J.; Castellanos-Gomez, A.; Late, D. J. Temperature-Dependent Raman Spectroscopy of Titanium Trisulfide (TiS_3) Nanoribbons and Nanosheets. *ACS Appl. Mater. Interfaces* **2015**, *7*, 24185−24190.
(22) Wu, K.; Torun, E.; Sahin, H.; Chen, B.; Fan, X.; Pant, A.; Parsons Wright, D.; Aoki, T.; Peeters, F. M.; Soignard, E.; Tongay, S. Unusual Lattice Vibration Characteristics in Whiskers of the Pseudo-One- Dimensional Titanium Trisulfide TiS_3. *Nat. Commun.* **2016**, *7*, 12952.
(23) Panda, S. K.; Datta, A.; Sinha, G.; Chaudhuri, S.; Chavan, P. G.; Patil, S. S.; More, M. A.; Joag, D. S. Synthesis of Well-Crystalline GaS Nanobelts and Their Unique Field Emission Behavior. *J. Phys. Chem. C* **2008**, *112*, 6240−6244.
(24) Ma, J. J.; Liu, X. Y.; Cao, X. J.; Feng, S. H.; Fleet, M. E. Bundle of Nanobelts Up to 4 cm in Length: One-Step Synthesis and Preparation of Titanium Trisulfide (TiS_3) Nanomaterials. *Eur. J. Inorg. Chem.* **2006**, *3*, 519.
(25) Wu, X. C.; Tao, Y. R.; Gao, Q. X. Preparation and field emission properties of titanium polysulfide nanobelt films. *Nano Res.* **2009**, *2*, 558−564.
(26) Li, G. H.; Jiang, Y.; Zhang, Y. G.; Lan, X. Z.; Zhai, T. Y.; Yi, G. C. High-Performance Photodetectors and Enhanced Field-Emission of CdS Nanowire Arrays on CdSe Single-Crystalline Sheets. *J. Mater. Chem. C* **2014**, *2*, 8252−8258.
(27) Chen, Z. G.; Cheng, L.; Zou, J.; Yao, X.; Lu, G. Q.; Cheng, H. M. Zinc sulfide nanowire arrays on silicon wafers for field emitters. *Nanotechnology* **2010**, *21*, No. 065701.
(28) Shang, N. G.; Meng, F. Y.; Au, F. C. K.; Li, Q.; Lee, C. S.; Bello, I.; Lee, S. T. Fabrication and Field Emission of High-Density Silicon Cone Arrays. *Adv. Mater.* **2002**, *14*, 1308−1311.
(29) Khare, R.; Shinde, D. B.; Bansode, S.; More, M. A.; Majumder, M.; Pillai, V. K.; Late, D. J. Graphene nanoribbons as prospective field emitter. *J. Appl. Phys. Lett.* **2015**, *106*, 23111.
(30) Song, Z.; Lei, H.; Li, B.; Wang, H.; Wen, J.; Li, S.; Fang, G. Enhanced field emission from in situ synthesized 2D copper sulfide nanoflakes at low temperature by using a novel controllable solvothermal preferred edge growth route. *Phys. Chem. Chem. Phys.* **2015**, *17*, 11790−11795.
(31) Suryawanshi, S. R.; Singh, A. K.; Deo, M.; Late, D. J.; Sinha, S.; More, M. A. 3D Hetero-architecture of GdB_6 nanoparticles on lessened cubic Cu_2O nanowires: enhanced field emission behaviour. *CrystEngComm* **2015**, *17*, 3936.
(32) Late, D. J.; More, M. A.; Misra, P.; Singh, B. N.; Kukreja, L. M.; Joag, D. S. Field Emission Studies of Pulsed Laser Deposited LaB_6 Films on W and Re. *Ultramicroscopy* **2007**, *107*, 825−832.
(33) Zhang, H.; Jimbo, Y.; Niwata, A.; Ikeda, A.; Yasuhara, A.; Ovidiu, C.; Kimoto, K.; Kasaya, T.; Miyazaki, H.; Tsujii, N.; Wang, H. High-endurance micro-engineered LaB_6 nanowire electron source for high-resolution electron microscopy. *Nat. Nanotechnol.* **2021**, *8*, 1−6.

https://doi.org/10.1021/acsanm.2c03460
ACS Appl. Nano Mater. 2023, 6, 44−49